Selective-mode optical nanofilters based on plasmonic complementary split-ring resonators

Iman Zand, Amirreza Mahigir, Tavakol Pakizeh,* and Mohammad S. Abrishamian

Faculty of Electrical and Computer Engineering, K. N. Toosi University of Technology, Tehran 16314, Iran
**T.Pakizeh@eetd.kntu.ac.ir*

Abstract: A nanoplasmonic optical filtering technique based on a complementary split-ring resonator structure is proposed. The basic and modal properties of the square-nanoring are studied using the group theory. Degeneracy and non-degeneracy of the possible TM odd- and even-modes are characterized based on the symmetry elements of the ring structure. Distinctively, the proposed technique allows selecting and exciting the proper plasmonic modes of the nanoring in the side-coupled arrangement. It is found that the non-integer modes can be excited due to the presence of a metallic nano-wall. These modes are highly sensitive to the nano-wall dimensions, in contrast to the regular integer modes. Moreover, the transmission-line theory is used to derive the resonance condition of the modes. The results show the optical transmission spectrum of the investigated filter can be efficiently modified and tuned either by manipulation of the position or by variation of the width of the employed nano-wall inside the ring. The numerical results support the theoretical analysis.

OCIS codes: (240.6680) Surface plasmons; (230.7400) Waveguides; (130.7408) Wavelength filtering devices; (130.3120) Optical resonators; (250.5300) Photonic integrated circuits.

References and links

1. R. Zia, J. A. Schuller, A. Chandran, and M. L. Brongersma, "Plasmonics: the next chip-scale technology," Mater. Today **9**(7-8), 20–27 (2006).
2. E. Ozbay, "Plasmonics: merging photonics and electronics at nanoscale dimensions," Science **311**(5758), 189–193 (2006).
3. G. Veronis and S. Fan, "Modes of subwavelength plasmonic slot waveguides," Opt. Express **16**, 2129–2140 (2008).
4. W. Cai, W. Shin, S. Fan, and M. L. Brongersma, "Elements for plasmonic nanocircuits with three-dimensional slot waveguides," Adv. Mater. (Deerfield Beach Fla.) **22**(45), 5120–5124 (2010).
5. D. F. P. Pile, T. Ogawa, D. K. Gramotnev, Y. Matsuzaki, K. C. Vernon, K. Yamaguchi, T. Okamoto, M. Haraguchi, and M. Fukui, "Two-dimensionally localized modes of a nanoscale gap plasmon waveguide," Appl. Phys. Lett. **87**(26), 261114 (2005).
6. G. Veronis and S. Fan, "Bends and splitters in metal-dielectric-metal subwavelength plasmonic waveguides," Appl. Phys. Lett. **87**(13), 131102 (2005).
7. J. A. Dionne, L. A. Sweatlock, H. A. Atwater, and A. Polman, "Plasmon slot waveguides: towards chip-scale propagation with subwavelength-scale localization," Phys. Rev. B **73**(3), 035407 (2006).
8. H. Gao, H. Shi, C. Wang, C. Du, X. Luo, Q. Deng, Y. Lv, X. Lin, and H. Yao, "Surface plasmon polariton propagation and combination in Y-shaped metallic channels," Opt. Express **13**(26), 10795–10800 (2005).
9. S. I. Bozhevolnyi, V. S. Volkov, E. Devaux, J. Y. Laluet, and T. W. Ebbesen, "Channel plasmon subwavelength waveguide components including interferometers and ring resonators," Nature **440**(7083), 508–511 (2006).
10. H. Zhao, X. Guang, and J. Huang, "Novel optical directional coupler based on surface plasmon polaritons," Physica E **40**(10), 3025–3029 (2008).
11. Y. Matsuzaki, T. Okamoto, M. Haraguchi, M. Fukui, and M. Nakagaki, "Characteristics of gap plasmon waveguide with stub structures," Opt. Express **16**(21), 16314–16325 (2008).
12. X. S. Lin and X. G. Huang, "Tooth-shaped plasmonic waveguide filters with nanometeric sizes," Opt. Lett. **33**(23), 2874–2876 (2008).
13. J. Tao, X. G. Huang, X. Lin, Q. Zhang, and X. Jin, "A narrow-band subwavelength plasmonic waveguide filter with asymmetrical multiple-teeth-shaped structure," Opt. Express **17**(16), 13989–13994 (2009).

#160870 - $15.00 USD Received 4 Jan 2012; revised 4 Mar 2012; accepted 4 Mar 2012; published 19 Mar 2012

14. J. Tao, X. G. Huang, and J. H. Zhu, "A wavelength demultiplexing structure based on metal-dielectric-metal plasmonic nano-capillary resonators," Opt. Express **18**(11), 11111–11116 (2010).
15. A. Noual, A. Akjouj, Y. Pennec, J.-N. Gillet, and B. Djafari-Rouhani, "Modeling of two-dimensional nanoscale Y-bent plasmonic waveguides with cavities for demultiplexing of the telecommunication wavelengths," New J. Phys. **11**(10), 103020 (2009).
16. X. Mei, X. Huang, J. Tao, J. Zhu, Y. Zhu, and X. Jin, "A wavelength demultiplexing structure based on plasmonic MDM side-coupled cavities," J. Opt. Soc. Am. B **27**(12), 2707–2713 (2010).
17. G. Wang, H. Lu, X. Liu, D. Mao, and L. Duan, "Tunable multi-channel wavelength demultiplexer based on MIM plasmonic nanodisk resonators at telecommunication regime," Opt. Express **19**(4), 3513–3518 (2011).
18. H. Lu, X. M. Liu, D. Mao, L. R. Wang, and Y. K. Gong, "Tunable band-pass plasmonic waveguide filters with nanodisk resonators," Opt. Express **18**(17), 17922–17927 (2010).
19. F. Hu, H. Yi, and Z. Zhou, "Wavelength demultiplexing structure based on arrayed plasmonic slot cavities," Opt. Lett. **36**(8), 1500–1502 (2011).
20. S. S. Xiao, L. Liu, and M. Qiu, "Resonator channel drop filters in a plasmon-polaritons metal," Opt. Express **14**(7), 2932–2937 (2006).
21. A. Hosseini and Y. Massoud, "Nanoscale surface plasmon based resonator using rectangular geometry," Appl. Phys. Lett. **90**(18), 181102 (2007).
22. T. Holmgaard, Z. Chen, S. I. Bozhevolnyi, L. Markey, and A. Dereux, "Dielectric-loaded plasmonic waveguide-ring resonators," Opt. Express **17**(4), 2968–2975 (2009).
23. Z. Han, V. Van, W. N. Herman, and P. T. Ho, "Aperture-coupled MIM plasmonic ring resonators with sub-diffraction modal volumes," Opt. Express **17**(15), 12678–12684 (2009).
24. T. B. Wang, X. W. Wen, C. P. Yin, and H. Z. Wang, "The transmission characteristics of surface plasmon polaritons in ring resonator," Opt. Express **17**(26), 24096–24101 (2009).
25. B. Yun, G. Hu, and Y. Cui, "Theoretical analysis of a nanoscale plasmonic filter based on a rectangular metal-insulator-metal waveguide," J. Phys. D Appl. Phys. **43**(38), 385102 (2010).
26. J. Liu, G. Fang, H. Zhao, Y. Zhang, and S. Liu, "Plasmon flow control at gap waveguide junctions using square ring resonators," J. Phys. D Appl. Phys. **43**(5), 055103 (2010).
27. T. D. Corrigan, P. W. Kolb, A. B. Sushkov, H. D. Drew, D. C. Schmadel, and R. J. Phaneuf, "Optical plasmonic resonances in split-ring resonator structures: an improved LC model," Opt. Express **16**(24), 19850–19864 (2008).
28. C. Rockstuhl, T. Zentgraf, T. P. Meyrath, H. Giessen, and F. Lederer, "Resonances in complementary metamaterials and nanoapertures," Opt. Express **16**(3), 2080–2090 (2008).
29. M. Navarro-Cía, M. Aznabet, M. Beruete, F. Falcone, O. El Mrabet, M. Sorolla, and M. Essaaidi, "Stacked complementary metasurfaces for ultraslow microwave metamaterials," Appl. Phys. Lett. **96**(16), 164103 (2010).
30. Y. Dong and T. Itoh, "Substrate Integrated Waveguide Loaded by Complementary Split-Ring Resonators for Miniaturized Diplexer Design," IEEE Microw.Wirel. Compon. Lett. **21**(1), 10–12 (2011).
31. G. Kumar, A. Cui, S. Pandey, and A. Nahata, "Planar terahertz waveguides based on complementary split ring resonators," Opt. Express **19**(2), 1072–1080 (2011).
32. S. F. A. Kettle, *Symmetry and Structure: Readable Group Theory for Chemists*, 3rd ed. (Wiley, 2007).
33. A. Taflove and S. C. Hagness, *Computational Electrodynamics: The Finite-Difference Time-Domain Method* (Artech House, Norwood, MA, 2005).
34. Z. H. Han, E. Forsberg, and S. He, "Surface plasmon Bragg gratings formed in metal-insulator-metal waveguides," IEEE Photon. Technol. Lett. **19**(2), 91–93 (2007).
35. R. F. Harrington, *Time-Harmonic Electromagnetic Fields* (IEEE Press, 2001).
36. D. M. Pozar, *Microwave Engineering*, 2nd ed. (Wiley, New York, 1998).
37. A. Alu, M. Young, and N. Engheta, "Design of nanofilters for optical nanocircuits," Phys. Rev. B **77**(14), 144107 (2008).

1. Introduction

Outstanding properties of plasmonic components such as their ability to highly confine optical waves below the diffraction limit and low bending-loss have made these structures a prime candidate for miniaturized photonic integrated circuits [1,2]. Great potential of plasmonic guiding nanostructures for high integration have motivated significant activities to explore their characteristics. Among those structures, the MIM configuration has attracted much interest due to its unique characteristics such as strong localization and ease of fabrication [3–7]. Different optical components such as Y-shaped combiners [8], Mach-Zehnder interferometers [9], and couplers [10] have been designed and demonstrated.

In recent years, plasmonic resonators have been subject of numerous studies. In this regard, the plasmonic stubs [11–13], nano-capillary resonators [14], side-coupled Fabry–Perot [15, 16], and slot cavities [17–19] have been investigated. These structures which generally are used for manipulating optical waves have been successfully employed as the efficient

#160870 - $15.00 USD Received 4 Jan 2012; revised 4 Mar 2012; accepted 4 Mar 2012; published 19 Mar 2012

components to achieve key optical devices such as wavelength demultiplexing structures [14–17, 19], band-stop and band-pas filters [11–13, 18]. One type of plasmonic resonators is ring resonator structure which generally possesses circular or rectangular geometries. Plasmonic band-stop filters based on the circular and rectangular ring resonators have been introduced in [20] and [21], respectively. Consequently, the band-stop [22, 23] and band-pass [24, 25] filters have been proposed based on the end-coupled and side-coupled arrangements. In addition, an optical add-drop coupler based on the square ring has been suggested [26].

In this contribution, we propose a novel optical filter design based on the complementary split-ring resonator (CSRR) in the side-coupled arrangement. In this design, a metallic nano-wall is positioned inside a MIM square-ring, resulting in a complement structure to the well-known split-ring resonators (SRR) [27–31]. By proper positioning of the wall, a resonance mode can be remarkably suppressed or excited. The different states of the resonance modes of the regular square ring are elaborated using the group theory [32] and principle of the perturbation. In this context, the symmetry arguments lead to modal descriptions of the CSRR structure. Moreover, we derive an analytical expression for the resonance condition of the proposed CSRR using the transmission line theory. Based on these descriptions, the influences of the nano-wall on the filtering characteristics are elucidated. Furthermore, the finite-difference time-domain (FDTD) method with the convolutional perfectly matched layer (CPML) boundary conditions [33] is used to numerically explore characteristics of the proposed filter. Both theoretical and simulation results demonstrate that not only specific resonance modes of the square nanoring can be selected by proper positioning of a metallic nano-wall, but also the interesting non-integer resonant modes are excited. However, these non-integer modes are not achievable by the regular ring. They are found to be highly sensitive to the nano-wall dimensions and simply can be manipulated by varying the width of the nano-wall. In contrary, the regular integer modes, in particular the high-order modes, show less sensitivity to the variations of the wall parameters.

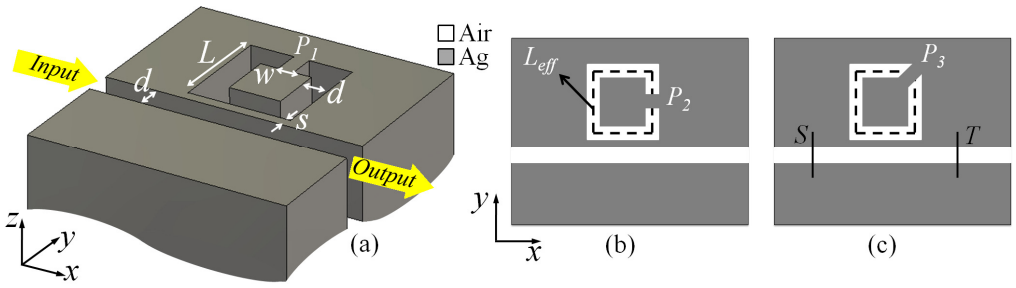

Fig. 1. Schematic of the proposed 2D plasmonic filter based on the CSRR structure including a metallic nano-wall placed in the position of (a) P_1, (b) P_2, and (c) P_3.

2. Modeling and theoretical analysis

Figure 1 shows the schematic of the proposed structure. The rectangular ring is surrounded by the metal (Ag) region. This ring is excited by a plasmonic channel waveguide, so-called bus-waveguide, in the side-coupled arrangement as shown in Fig. 1(a-c). The waveguide confines the exciting optical power in the insulator (air) region. Splitting the MIM square ring by adding a metallic nano-wall makes the structure a complement to the metallic SRR. In this study, the wall is placed in three positions, denoted by P_1 (Fig. 1(a)), P_2 (Fig. 1(b)), and P_3 (Fig. 1(c)). The main structural parameters of the filter are the width of the MIM waveguide (d), gap size between the bus-waveguide and the ring (s), side length of the ring (L), wave-guiding length in the ring (L_{eff}), and width of the nano-wall (w). To calculate transmittance of the filter ($T = P_{out} / P_{in}$) incident power of P_{in} and transmitted power of P_{out} are monitored at positions of S and T, respectively. The insulator is assumed to be air ($\varepsilon_i = 1$), and the complex

#160870 - $15.00 USD Received 4 Jan 2012; revised 4 Mar 2012; accepted 4 Mar 2012; published 19 Mar 2012

relative permittivity of silver $\varepsilon_m(\omega)$ is characterized by the Drude model: $\varepsilon_m(\omega) = \varepsilon_\infty - \omega_p^2 / (\omega^2 + i\gamma\omega)$, where $\varepsilon_\infty = 3.7$, $\omega_p = 9.1$ eV, and $\gamma = 0.018$ eV [34]. The width of the MIM waveguides (d) is set to be 50 nm to ensure that only the fundamental TM mode is supported. The complex propagation constant β of this waveguide mode can be obtained from solving the eigenvalue equation [7]:

$$\tanh\left(\frac{\gamma_i d}{2}\right) = -\frac{\varepsilon_i \gamma_m}{\varepsilon_m \gamma_i} \tag{1}$$

where γ_i and γ_m, the wave attenuation constants in the transverse direction, defined as $\gamma_i = \sqrt{\beta^2 - \varepsilon_i k_0^2}$ and $\gamma_m = \sqrt{\beta^2 - \varepsilon_m k_0^2}$; and ε_i, ε_m, k_0, and β are the dielectric constants of the insulator and the metal, wave number in free-space, and the propagation constant of the guided mode, respectively. In the simulations, the structure in the z direction is considered to be infinite (2D), schematically shown in Fig. 1(a). We note, however, for on-chip optical components, the structures should be made finite [3–5].

2.1 Square ring resonator

The resonance modes of a rectangular ring are often compared with the modes of a circular ring. In the side-coupled arrangement, it is expected that a rectangular ring couples more efficiently to a bus-waveguide, compared to a circular ring. Another feature is that in contrast to a circular ring, a rectangular ring may exhibit new resonance modes because of its certain geometrical symmetry. Generally speaking, the possible differences in their transmission spectra are mainly attributed to the role of the corners of a rectangular ring structure [21, 26]. In this section, we investigate the effects of the corners on the resonance modes of the square ring in more details using the group theory and the principle of perturbation. Hence, physical origins of the effects are discussed. This enables us to theoretically study the modes of the CSRRs.

Since the geometrical symmetry of the resonators and their resonance modes are related to each other, the group theory can be illustrative to explore and predict the resonance properties of the square ring. Based on this theory, it can be shown that square ring resonator possesses symmetry of C_{4v} [32]. In general, for symmetry group of C_{nv}, $2\pi/n$ is the smallest angel of rotation which causes the pattern to appear unchanged and index of "v" indicates the existence of symmetry planes. Considering the magnetic fields as a base for the modal description, the resonance modes of the square ring can be classified and described based on the character table of C_{4v} and the corresponding symmetry elements of the structure. Accordingly, there is five mode classes indicated by $TM_{(4k)c}$, $TM_{(4k)f}$, $TM_{(4k-2)f}$, $TM_{(4k-2)c,}$ and $TM_{(2k-1)}$ (k = 1, 2, ...), in which the even modes can be generally categorized as either a corner-mode (TM_{mc}) or a face-mode (TM_{mf}). Although the odd resonances modes TM_n (n = $2k$-1) possess two fold degeneracy, the even modes TM_m (m = $2k$) are non-degenerate. Comparing the circular and square ring geometries, the corners of the square ring can be treated as outward perturbations of the circular structure. Therefore, the perturbations effects, caused by the corners, on the resonance modes should be considered. In this sense, positions of the corners with respect to the symmetry planes are playing important role. Since the perturbations caused by the corners equally affect the odd degenerate resonance pairs, their degeneracy is not lifted. In contrast, the corners influence differently the $TM_{(4k)c}$ and $TM_{(4k)f}$ modes. This results in a splitting of these modes into two distinct resonances. Thus the resonance wavelengths of the face- and corner-modes deviate from their primary values, obtained for a regular circular ring. These deviations can be expressed by [35]:

$$\Delta\omega / \omega_0 \approx (\Delta W_m - \Delta W_e) / W \tag{2}$$

#160870 - $15.00 USD Received 4 Jan 2012; revised 4 Mar 2012; accepted 4 Mar 2012; published 19 Mar 2012

where W denotes the total energy stored in the original cavity, and ω_0 is angular frequency of the modes of even pairs when they are still degenerate. ΔW_m and ΔW_e denote the time-averaged magnetic- and electric-energy, originally stored in the small volume ΔV, respectively. Based on Eq. (2) and the field distributions of the TM_{mc} and TM_{mf} modes, it is predictable which mode resonates in the longer wavelength. The outward perturbation will increase (decrease) the resonance frequency if it is created at the position of a large electric (magnetic) field. Thus, the TM_{mc} modes always resonate at longer wavelengths in comparison with the TM_{mf} modes. In this sense, the corresponding stored energies of each mode in the corners should be taken into account. Otherwise, it is almost unpredictable which mode deviates more from the values obtained by the conventional analytical formula of the square ring, i.e. $L = N \lambda_g$, where N, an integer, is the mode number. Moreover, by increasing the mode number of the TM_{mc} and TM_{mf} modes: $\Delta W_m - \Delta W_e \approx 0$; thereby their resonance wavelengths approach to each other [21].

Unlike the end-coupled square ring [25], all corner- and face-modes of the square ring can be excited in the side-coupled arrangement. For an isolated square ring the two odd resonant (TM_n) modes are degenerate, exhibiting a single resonance. However, the bus-waveguide breaks the symmetry of the structure, and as a result the degeneracy is lifted. Hence, the degenerate modes coupled to each other, and the modes split to two modes. One mode (TM_n^s) is symmetric with respect to the symmetry plane of the whole structure, and the other mode (TM_n^a) is asymmetric. These modes cannot be distinguished in the transmission spectrum of a side-coupled square ring because of the weak splitting of the modes and the relatively low Q-factor of the plasmonic resonators. Thus, it is expected that the odd modes have wider bandwidth in comparison with the even modes. Moreover, the traveling-wave (TW) characteristic of the odd resonances reported in [26] is possibly due to the excitation of the standing-wave TM_n^s and TM_n^a modes which are out-of-phase. It should be emphasized that the TM_n^s and TM_n^a modes become degenerate by removing the bus-waveguide.

2.2 Complementary SRR: CSRR

According to the above discussion, by placing a metallic nano-wall on the symmetry planes of the square ring one can manipulate only one of the TM_{mc} or TM_{mf} mode classes and thereby can modify the transmission spectrum of the filter. For this purpose, in here three proper positions for the wall are considered which are located in the corner and middle of the square faces of the ring, as shown in Fig. 1(a)-1(c). Since the minima of the electric field occur on the both sides of the metallic wall, a resonance mode may be drastically manipulated, depending on weather the wall is placed in the antinodes of magnetic fields (nodes of electric fields) or not. In fact, for the resonance modes, an antinode of the magnetic field (or node of the electric field) can be treated as an equivalent electrical short-circuit. Thus, by placing the nano-wall in the defined position P_1 or P_2, the TM_{mc} modes are suppressed, but for the wall placed in the position P_3, the TM_{mf} modes are suppressed. Moreover, the metallic nano-wall placed in the position P_1 or P_2 suppresses one of the TM_n^a and TM_n^s modes, respectively. Although, for the position P_3, a new mode ($TM_1(P_3)$) can be created which is neither TM_n^a mode nor TM_n^s mode. The antinode of the magnetic field of this mode is located on the symmetry plane of the ring.

Comparing structures of the proposed plasmonic CSRR and MIM cavity [16] indicates that the CSRR can be considered as a closed straight cavity which is bent, and its ends are separated by the wall. Based on this analogy the CSRR can support both the integer modes (including even number of antinodes) and the non-integer modes (including odd number of antinodes). The square ring, in contrary, only supports the integer modes [21, 25, 26]. In the CSRR, there are two possible arrangements for the magnetic fields on the sides of the wall.

#160870 - $15.00 USD Received 4 Jan 2012; revised 4 Mar 2012; accepted 4 Mar 2012; published 19 Mar 2012

They can be either with the same (integer modes) or opposite (non-integer modes) polarities on the sides of the wall. There is an important phenomenon which brings about a special characteristic for the non-integer modes in comparison with the integers modes. This phenomenon can be understood by comparing the polarities of the magnetic fields on the sides of the wall for the both types of modes. Particularly, in the non-integer modes opposite polarity of the magnetic fields on the sides of the wall indicates flow of co-directional electrical currents in the wall. On the other side, for the integer modes, two contra-directional current excited in the wall cancel each other out. Based on this behavior it can be concluded that, for the non-integer modes, the metallic nano-wall acts like a nanoinductor. Thus, the non-integer modes become highly sensitive to dimensions of the wall. Moreover, based on the symmetry arguments, the anti-nodes of the non-integer modes can be altered by changing position of the nano-wall.

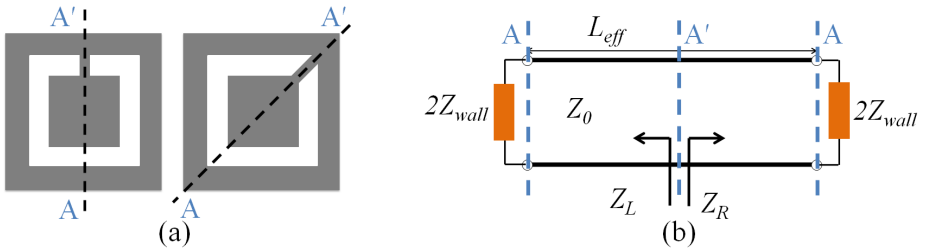

Fig. 2. (a) Schematics of the isolated CSRRs with their symmetry plane (AA') for the nano-wall placed in the middle of the face and corner. (b) The transmission-line model of the CSRR.

The resonance condition of the CSRR structure can be obtained by employing the transmission line theory. The schematic of the transmission line resonator model of the integer and non-integer modes of the CSRR is shown in Fig. 2(b). Symmetry plane (AA') of the resonator is also plotted for the clarity. The input impedance seen from the left (Z_L) and right (Z_R) side of the symmetry plane can be simply expressed by [36]:

$$Z_L = Z_R = Z_0 \frac{2Z_{wall} + iZ_0 \tan(\beta L_{eff}/2)}{Z_0 + i2Z_{wall} \tan(\beta L_{eff}/2)} \qquad (3)$$

where L_{eff} is the wave-guiding length in the ring as shown in Fig. 1, and Z_{wall} is the impedance of the nano-wall. Due to the inductance behavior of the nano-wall its equivalent impedance can be expressed by $Z_{wall} = -i\omega d/(\omega^2 \varepsilon_m(\omega) w)$, where w and d are the width and length of the inductance, respectively [37]; and $\varepsilon_m(\omega)$ is the permittivity of the wall made of the silver. The characteristic impedance of the MIM waveguide in each section is denoted by Z_0, shown in Fig. 2(b), and it can be expressed by $Z_0 = \beta d/\omega\varepsilon_0$ [6]. The values of β can be obtained by solving Eq. (1). Since the resonator is symmetrical, at the midpoint of the line, the resonance condition required that $Z_R = Z_L^* = Z_L$, or simply $\mathrm{Im}\{Z_L\} = 0$. By employing this condition, the resonance wavelengths of the modes can be obtained. It should be pointed that the mentioned condition is true when the metal loss is ignored and hence β is real. For the complex β (lossy metals) minimums of $\mathrm{Im}\{Z_L\}$ should be found. In the case of the integer modes, the nano-wall is placed where the equivalent short-circuit of these modes exist. Moreover, as mentioned earlier, the integer modes do not support co-directional flow of the currents in the wall. Hence, by applying $Z_{wall} \approx 0$ the resonance condition of the integer modes can be obtained. In special case in which β is real, the resonance condition would be '$\tan(\beta L_{eff}/2) = 0$' (or $\beta L_{eff} = 2N\pi$) where N, an integer, is the mode number of an integer mode. The described condition is similar to the resonance condition of the rectangular ring

#160870 - $15.00 USD Received 4 Jan 2012; revised 4 Mar 2012; accepted 4 Mar 2012; published 19 Mar 2012

proposed in [21]. The only difference is the effective length of the resonator which is decreased by the width of the wall. Therefore, it is expected that resonance wavelengths of the integer modes of the CSRR to be similar to the corresponding modes of the regular ring. However, the position and width of the wall should be properly considered.

3. Simulation results and discussions

3.1 Integer and non-integer modes

The transmission spectra of the proposed filter are plotted in Fig. 3. These spectra are compared with the transmission spectrum of the regular square ring (Fig. 3(a)). The magnetic-field distributions of the resonance modes are shown as insets in Fig. 3. To study the effects of the position of the wall on the response of the filter, three cases are considered. First, the wall is placed at the position P_1 (Fig. 3(b)). The spectrum clearly depends on the position of the wall (see Fig. 3(b)-3(d)). The structural parameters of the filter are set to be L = 300 nm, d = 50 nm, s = 20 nm, and w = 20 nm. A resonance mode of a regular square-ring is denoted by TM_y whereas a resonance mode of the CSRR is denoted by $TM_y(P_x)$, where "P_x" and "y" stand for the position of the wall and type of the mode, respectively. It is observed that resonance wavelength of the TM_{2c} mode is longer than that of the TM_{2f} mode as can be explained by the principle of perturbation. Additionally, the longer resonance wavelength of the $TM_1(P_1)$ mode, compared with the $TM_1(P_2)$ and $TM_1(P_3)$ modes, can be attributed to the perturbation caused by the bus-waveguide. Since the bus waveguide perturbs the middle and corners of the lower branch of the ring differently, the resonance wavelengths of $TM_1(P_2)$ and $TM_1(P_3)$ modes are close but different from the resonance wavelength of $TM_1(P_1)$ mode. This behavior can be seen in Fig. 3(b)-3(d), the magnetic fields of the $TM_1(P_2\text{-}P_3)$ modes in the lower branch are more concentrated in the corners rather than the middle-part. While, the field associated with the $TM_1(P_1)$ mode are concentrated in the middle-part of the branch. As seen in Fig. 3, in addition to the regular modes of the square ring, extra drops are seen in the transmission spectra of the CSRR for different positions of the wall. The magnetic-field distributions of these extra drops show these modes are the non-integer modes as predicted in the previous section. Characteristics of these non-integer modes are investigated in the following sections.

#160870 - $15.00 USD Received 4 Jan 2012; revised 4 Mar 2012; accepted 4 Mar 2012; published 19 Mar 2012

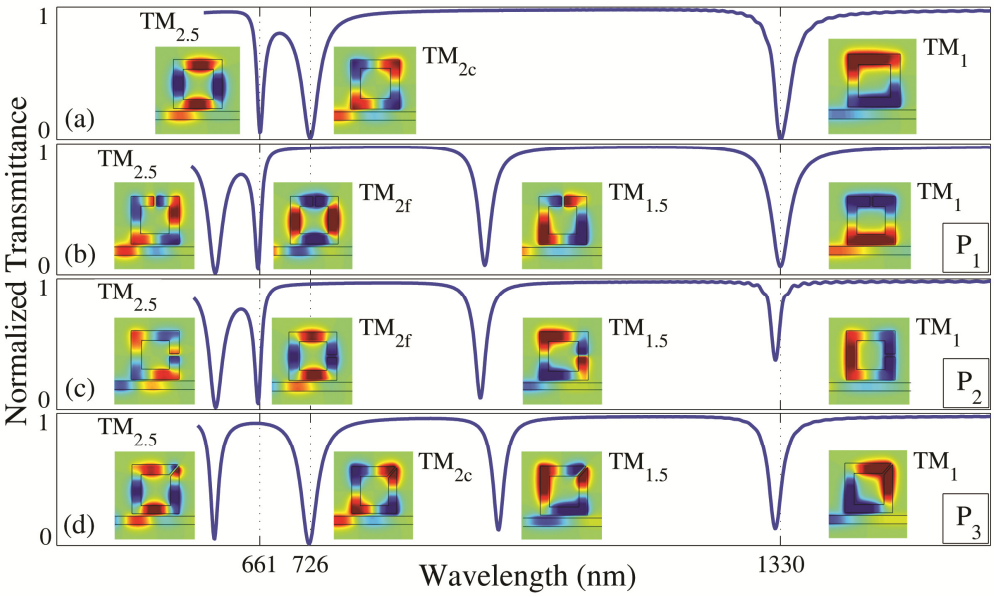

Fig. 3. Transmission spectrum of the filter comprises a regular square ring with L = 300 nm (a), and the spectra of the proposed CSRR filter with a nano-wall placed in position P_1 (b), P_2 (c), and P_3 (d), calculated using the FDTD method. In all cases w = 20 nm. The magnetic-field distributions at the resonance wavelengths are shown as insets.

3.2 Effects of the position of the nano-wall

Manipulating the transmission spectra of the CSRRs by exciting or suppressing the TM_{2c} or TM_{2f} modes of the regular ring is one of the features of incorporating the nano-wall inside the ring. According to Fig. 3, for the cases that the wall is placed in the positions P_1 and P_2, TM_{2c} is severely suppressed. However, the TM_{2f} mode is suppressed if the wall is placed in P_3. Comparing the resonance wavelengths and the field profiles of the TM_{2c} and TM_{2f} modes with the $TM_{2c}(P_3)$ and $TM_{2f}(P_1\text{-}P_2)$ modes shows that unaffected even modes are almost the same as their counterpart modes in the regular ring structure. This behavior is in accordance with the theoretical descriptions presented in Sec. 2. In contrast, the first resonance of the ring $TM_1(P_i)$ is not suppressed for all of P_1, P_2, and P_3 positions. For the case with the wall placed in P_1 (P_2), the TM_{1a} (TM_{1s}) mode is suppressed, and the TM_{1s} (TM_{1a}) mode remains unaffected. By positioning the wall in P_3, a resonance mode ($TM_1(P_3)$) which possesses the antinodes of the magnetic field in the corners is excited. In this case, the optical power guided by the bus-waveguide can couple to the ring from the corners.

Comparing the mode profiles of the resonance modes shown in Fig. 3 reveals another interesting feature of incorporating the metallic nano-wall. Expectedly, the antinodes of the field patterns can be manipulated by the position of the wall. The importance of this phenomenon can be understood by the fact that in the MIM configuration, the efficient extraction of optical power from a resonator occurs when the extracting waveguide is in the position of antinodes of the magnetic fields. In the previous section, based on the group theory, we concluded that the odd resonances of the square ring possess two degenerate modes, which split by the side-coupled arrangement and form two symmetric and asymmetric modes. One of the main advantages of utilizing the nano-wall is to selectively excite or suppress one of these modes. Furthermore, for the case with the wall in P_3 the CSRR still possesses symmetry of C_{1v} [32], which forces the antinodes of the field profile of the fundamental mode to be located on the symmetry plane of the structure. It is observed that non-integer modes, especially the fundamental mode, are remarkably altered by changing the position of the wall. Thus, the proposed structure offers more flexibility in arranging the

#160870 - $15.00 USD Received 4 Jan 2012; revised 4 Mar 2012; accepted 4 Mar 2012; published 19 Mar 2012

output ports. For instance, the $TM_1(P_1)$ mode can be extracted by an output port which is perpendicular to the bus-waveguide, but the $TM_1(P_2)$ mode can be extracted by a port which is parallel to the bus-waveguide. Moreover, comparing the characteristics of the non-integer modes indicates that the resonance wavelengths of the low-order modes are influenced more than the high-order modes. For example, variation of the resonance wavelength by changing the position of the wall for $N = 1.5$ is about 15 nm, while for $N = 2.5$ is negligible.

3.3 Tunability of the resonances: Effects of the width of the nano-wall

The transmission spectra of the proposed CSRRs are remarkably influenced by the nano-wall. Thus, its role on the transmission spectrum and, in particular, the resonance wavelengths of the structure is numerically studied. Figure 4 shows dependence of the resonance wavelengths of the integer and non-integer modes on the width of the wall, *w*. The structural parameters of the resonator are kept the same as in Fig. 3, and *w* varies from 10 to 50 nm. Generally, the resonance wavelengths of the considered modes decrease by increasing the width *w*. However, there is a distinct dissimilarity between the integer and non-integer modes which should be pointed out. As shown in Fig. 4(a), maximum variations in the resonance wavelengths of the $TM_1(P_1\text{-}P_3)$ modes are about 23 nm, 24 nm, and 37 nm, respectively. Similarly, according to the Fig. 4(c), maximum variations in the resonance wavelengths of the $TM_{2c}(P_3)$ and $TM_{2f}(P_1\text{-}P_2)$ modes are almost 16 nm and 11 nm, respectively. In contrast, the resonance wavelengths of the non-integer modes, i.e. $TM_{1.5}(P_1\text{-}P_3)$ and $TM_{2.5}(P_1\text{-}P_3)$, vary about 116 nm and 70 nm while the width *w* varies from 10 to 50 nm (Fig. 4(b), 4(c)). Thus, in comparison with the integer modes, the non-integer modes are highly sensitive to variation of *w*. The drastic different behaviors of the non-integer and integer modes can be attributed to the inductive behavior of the metallic nano-wall for the non-integer modes. In accordance with the numerical results, a large inductive behavior of a narrow metallic wall may result in a large change in the resonant wavelengths. Nevertheless, the equivalent inductance is smaller for the wider wall. Moreover, the results show that sensitivity of the resonance wavelengths of the both integer and non-integer modes to the variation of *w* decreases by increasing the mode number (Fig. 4). The numerically calculated resonance wavelengths of the CSRR are compared with the theoretical results obtained using the analytical formula derived in Sec. 2. It is seen that the analytical results (dashed-line) are reasonably in a good agreement with the numerical results. Although the trends seen in the variation of the resonance wavelengths of the modes are similar, the small quantitative discrepancies for the resonance modes might be noticed. These deviations are mainly attributed to the presence of the bus-waveguide near the resonator in the FDTD simulations. This causes a shift in the resonances. Furthermore, the deviation between the resonance wavelengths of the $TM_{2c}(P_3)$ and $TM_{2f}(P_1)$ modes, observed in Fig. 4(c), are because of the perturbations caused by the corners.

#160870 - $15.00 USD Received 4 Jan 2012; revised 4 Mar 2012; accepted 4 Mar 2012; published 19 Mar 2012

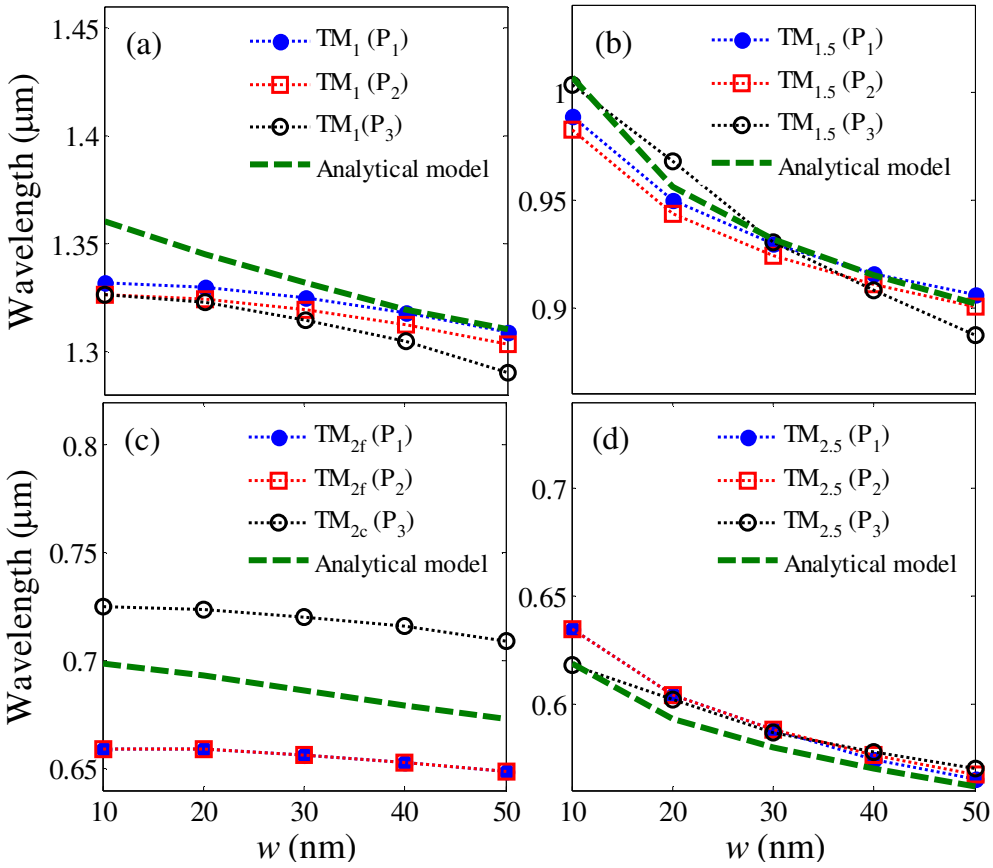

Fig. 4. Variations of the resonance wavelenghts of the CSRR versus the width of the wall, *w*, for the corresponding low-order integer and non-integer modes: (a) TM_1, (b) $TM_{1.5}$, (c) TM_2, and (d) $TM_{2.5}$, calculated by the FDTD method and the transmission-line theory.

4. Conclusion

In summary, a 2D plasmonic nanofilter designed based on the CSRR structure is proposed. The theoretical analysis and the numerical calculations demonstrate the mode-selectivity and the filtering tunability of the proposed structure. Interestingly, incorporating a metallic nano-wall within the MIM nanoring structure led to excitation of the non-integer modes. The results show these modes are highly tunable by manipulating the width of the nano-wall. The basic electromagnetic modes of the plasmonic CSRR are elaborated using the group theory. Moreover, the transmission-line theory is used to estimate the resonance wavelengths of the proposed structure. The band shift of ~120 nm is achieved for the fundamental mode of the CSRR upon a gradual variation of the width of the wall from 10 to 50 nm. The findings suggest the potential of our design for a tunable and compact optical nanofilter in integrated optical circuits and for nanophotonics applications.

#160870 - $15.00 USD Received 4 Jan 2012; revised 4 Mar 2012; accepted 4 Mar 2012; published 19 Mar 2012